NANO LETTERS

Letter

pubs.acs.org/NanoLett

Atomistic Near-Field Nanoplasmonics: Reaching Atomic-Scale Resolution in Nanooptics

M. Barbry,[†] P. Koval,[†] F. Marchesin,[†] R. Esteban,[†] A. G. Borisov,[‡] J. Aizpurua,*[,†] and D. Sánchez-Portal*[,†]

[†]Centro de Física de Materiales, Centro Mixto CSIC-UPV/EHU, and Donostia International Physics Center (DIPC), Paseo Manuel de Lardizabal 5, 20018 Donostia-San Sebastián, Spain

[‡]Institut des Sciences Moléculaires d'Orsay ISMO, UMR 8214 CNRS-Université Paris-Sud, Bât. 351, Université Paris-Sud, 91405 Orsay Cedex, France

Supporting Information

ABSTRACT: Electromagnetic field localization in nanoantennas is one of the leitmotivs that drives the development of plasmonics. The near-fields in these plasmonic nanoantennas are commonly addressed theoretically within classical frameworks that neglect atomic-scale features. This approach is often appropriate since the irregularities produced at the atomic scale are typically hidden in far-field optical spectroscopies. However, a variety of physical and chemical processes rely on the fine distribution of the local fields at this ultraconfined scale. We use time-dependent density functional theory and perform atomistic quantum mechanical calculations of the optical response of plasmonic nanoparticles, and their dimers, characterized by the presence of crystallographic planes, facets, vertices, and steps. Using sodium clusters as an example, we show that the atomistic details of the nanoparticles morphologies determine the presence of subnanometric near-field hot spots that are further enhanced by the action of the underlying nanometric plasmonic fields. This situation is analogue to a self-similar nanoantenna cascade effect, scaled down to atomic dimensions, and it provides new insights into the limits of field enhancement and confinement, with important implications in the optical resolution of field-enhanced spectroscopies and microscopies.

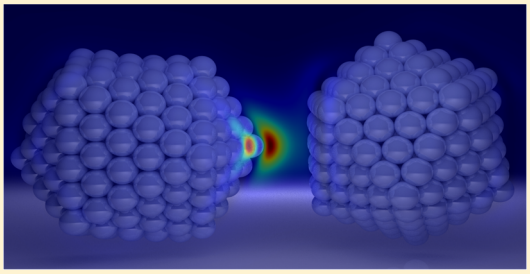

KEYWORDS: *Plasmonic nanoantennas, optical response, TDDFT, DFT ab initio calculations, field enhancement*

Metallic nanoparticles are key in the development of nanooptics. The ability of the conduction electrons to collectively oscillate produces surface charge density oscillations in nanoparticles, so-called surface plasmons, that couple very efficiently to light, producing subwavelength localization and large enhancement of the optical fields induced at the nanoparticles.[1−6] Nanooptics with localized surface plasmons has thus boosted a variety of technological applications in which the intense electromagnetic fields can assist in enhancing the signal from vibrational spectroscopies,[7−10] improving the performance of solar cells,[11,12] optimizing the active control of nanodevices,[13−16] or implementing noninvasive thermotherapies in medicine,[17] among others. In all of these applications, the optical response that determines the properties of plasmonic surface modes is typically determined in the framework of classical electrodynamics, by solving Maxwell's equations for a particular material, shape, size, and environment. In this way, for instance, plasmonic modes of spherical nanoparticles,[18,19] nanoshells,[20] nanorings,[21] nanorods,[22−25] nanostars,[26,27] dimers,[3,28,29] or particle oligomers[30,31] have been routinely estimated during the last years. The mode volumes typically reached in these structures are in the range of some tens of nanometers, and the actual degree of their field confinement is determined by the morphology of the nanostructure (curvature, thickness, interaction between different particles, etc.),[5,32−34] The effective squeezing of electromagnetic energy into these nanometric dimensions has triggered out referring to plasmonic nanostructures as optical nanoantennas.[35,36]

As nanotechnology reaches a control of nanoarchitectures at scales of the order of the nanometer and even subnanometer,[37−41] nanooptics is called to face new regimes of interaction, where the atomic scale needs to be considered to correctly determine the optical response of the nanosystem. Optical processes at the atomic scale can be critical in many branches of nanoscience such as in field-enhanced photochemistry,[42−45] in single molecule spectroscopy,[8,46−49] or in electronics at optical frequencies.[38,50−53]

Most of these situations require a complete theoretical framework that accounts for the quantum nature of the electrons in their interaction with light. Time-dependent density functional theory (TDDFT)[54,55] provides the adequate framework to tackle the optical response of plasmonic nanoantennas where the complex nonlocal screening,[56,57] the smooth electronic density profile at the metal interface,[58] quantum size effects,[59−61] and electron tunneling across

Received: February 24, 2015
Revised: April 22, 2015
Published: April 27, 2015

DOI: 10.1021/acs.nanolett.5b00759
Nano Lett. 2015, 15, 3410−3419

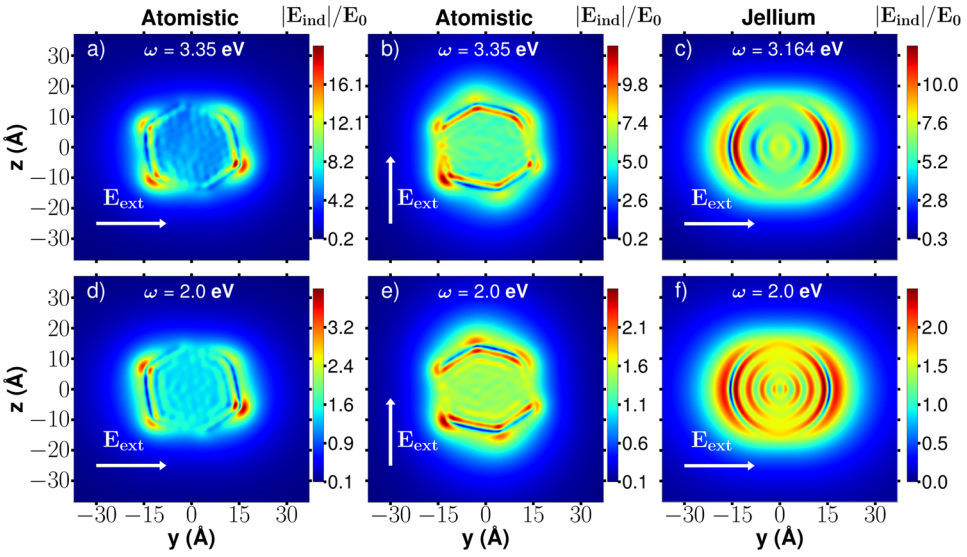

Figure 1. Induced-field enhancement, $|\mathbf{E}_{ind}|/\mathbf{E}_0$, with $\mathbf{E}_0$ the amplitude of the incident field, in the proximity of a Na_{380} cluster and a jellium sphere (r_s = 2.12 Å) of radius R = 15.57 Å. The induced field is represented in the (y, z) plane, that passes through the center of the cluster/sphere. Top panels show the results at the dipolar plasmonic excitation (at 3.35 and 3.16 eV, for the atomistic and jellium models, respectively), (a) for a polarization of the external field along the y axis, (b) along the z axis, and (c) along the y axis, (although the response is isotropic in the jellium case). Panels d−f show the same information as a−c for an energy of the exciting field out of resonance (2 eV). The orientation of the Na_{380} particle with respect to the coordinate axis is clarified in Figure S1 in the Supporting Information.

metallic nanogaps[62,63] can be properly considered. Furthermore, an atomistic description of the nanostructures[64] can address the effect in the optical response of atomic-scale features at the surfaces such as the presence of protruding atoms, steps, vertices, or edges at the contact of crystallographic planes. Although these atomic-scale effects might be sometimes masked in experimental far-field techniques, they are very relevant in spectroscopy techniques that directly rely on the ultrafine details of the near-field intensity and distribution.

Here we theoretically show how the atomic features at the surfaces of plasmonic nanoparticles do localize electromagnetic fields down to atomic-scale dimensions showing resonant (plasmonic) and nonresonant (lightning rod effect) field enhancements that alter the standard conception of localization of plasmonic fields. With help of our TDDFT calculations, we show near-field maps of plasmonic nanoparticles and their dimers, which produce atomic-scale hot spots superimposed to the plasmonic resonances. These are the atomic-scale analogue of the lightning rod effect,[65−67] which can also be understood as the atomistic limit of the classical field divergence at an infinitely sharp metallic tip. Indeed, the sharpest possible structure would be set by a vertex ending with a single atom. The quantum description of such system, where the nonlocal screening of conduction electrons is included,[68] sets a limit for the attainable field enhancement. However, when this effect is combined with the overall field enhancement given by a plasmon resonance, we show here that very intense and localized atomic-scale hot spots can be obtained. The presence of these hot spots has been proposed and even exploited experimentally in subnanometer-resolved surface-enhanced optical spectroscopies.[49,69−72] An accurate description of the physical properties of atomic-scale local near-fields has been elusive to date due to the limitations of classical and quantum descriptions that, even if capable of correctly reporting the main trends of the response, are typically based on strong approximations either on the electromagnetic boundary conditions or the atomic structure of surfaces. Our calculations provide a faithful description of the actual near-field induced in metallic interfaces considering realistic atomic structures, unambiguously resolving the near-field features at the hot spots with unprecedented resolution and detail. We can thus quantify the level of confinement of the near fields relevant in complex photochemical processes and near-field spectroscopies. Our results indicate that, at the vertices and edges formed at the contact of different facets, it is possible to localize plasmons with subnanometric resolution and beat the typical plasmonic confinement imposed by the nanoparticle size. Thus, similar to cluster and surface science where the distinct electronic properties of atoms at steps and edges between crystallographic facets have been extensively considered, e.g., in the context of reactivity,[73−76] the atomic-scale structure of plasmonic interfaces appears as a new arena of research. The extreme plasmon-localization reported here might allow to implement and exploit novel probes, capable to provide ultraresolution and reach access to information on single molecules.

We apply our atomistic calculations to obtain the optical response and the near-field distribution in a single Na_{380} cluster, as well as in dimers formed by two Na_{380} clusters. This is the largest cluster size for which the global minimum icosahedral symmetry (as described using an effective Murrell−Mottram potential[77]) is available.[78] We took this structure[79] as a starting point for further ab initio relaxation using density functional theory (DFT), as implemented in the SIESTA code,[80,81] within the local density approximation[82] (LDA). The resulting atomic structure of the Na_{380} cluster is very similar to the initial one, although it has a higher density due to the well-known underestimation of the sodium lattice parameter by LDA.[83] This result confirms that the selected structure is stable and at least corresponds to a local minimum of the DFT energy landscape of Na_{380}. Subsequently we obtained the TDDFT linear optical response of the cluster within the so-called adiabatic local density approximation, i.e., using the LDA exchange-correlation kernel. The calculations were performed

DOI: 10.1021/acs.nanolett.5b00759
Nano Lett. 2015, 15, 3410−3419

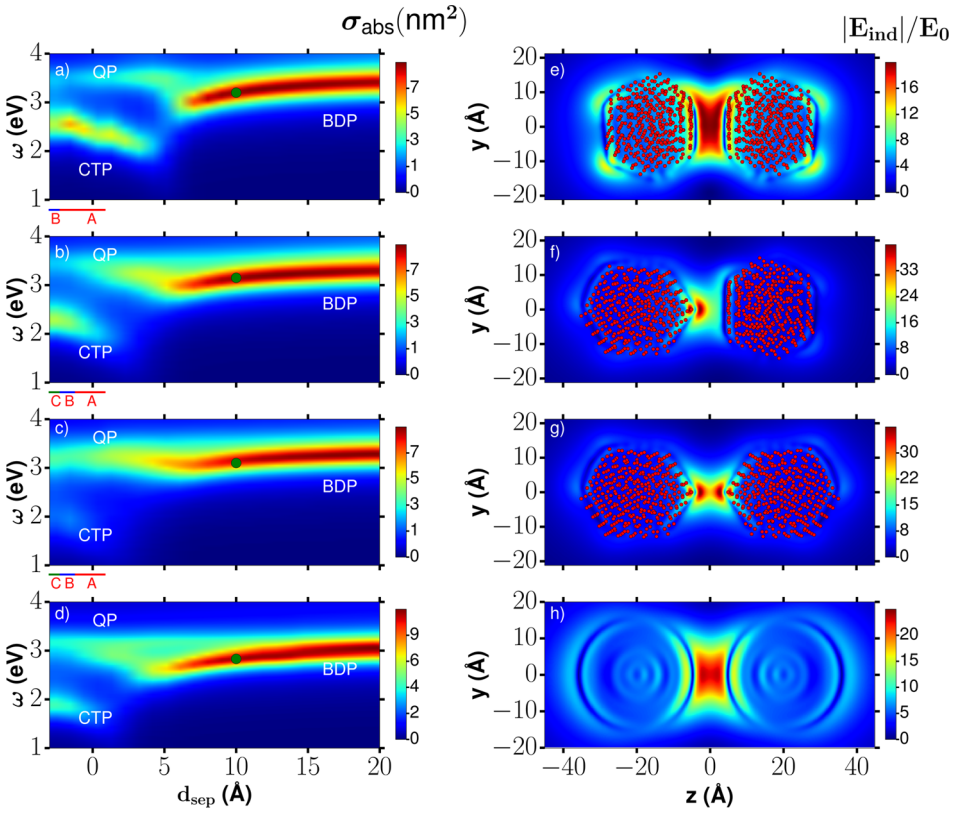

Figure 2. Panels a–d show the spectral evolution of the absorption cross-section of the plasmonic dimers depicted in e–g, and a dimer of jellium spheres (h), for a polarization of the incident field along the dimer axis as a function of separation distance between the particles, d_{sep}. The hybridized bonding dipolar plasmon (BDP), the charge-transfer plasmon (CTP) mode, and the quadrupolar plasmon (QP) model are identified in the spectra. Separation distances lower than 1 Å and negative distances represent overlapping clusters and have been modeled in a–c by modified geometries in which atomic layers of one of the clusters are subsequently removed (region A, one layer removed; region B, 2 layers; region C, 3 layers). Panels e–h show the distribution of the local induced-field produced in the (y,z) plane containing the axis of the dimer for an energy in resonance with the BDP and for a separation distance of 10 Å: (e) the gap is formed by a facet-to-facet junction, (f) facet-to-tip, and (g) tip-to-tip configurations. In (h) the same situation for a dimer described by the jellium model is displayed.

using an efficient iterative scheme[84−86] that allows to obtain the optical response at the TDDFT level for large clusters and molecules with moderate computational resources.[87] The technical details of the method can be found in the Supporting Information. The results of our atomistic simulations are compared to TDDFT-LDA simulations performed for Na clusters described within the jellium model (JM).[63] In the JM only the valence electrons are treated explicitly, and the ionic cores are represented through an homogeneous positive charge density bound by the cluster boundary (jellium edge). In the comparison, we use JM spheres of radius 15.57 Å and fix the averaged electron density to that of bulk Na (Wigner−Seitz radius r_s = 2.12 Å). The resulting closed-shell JM cluster contains 398 electrons and is similar in size to the Na_{380} cluster tackled in the atomistic calculations.

We first explore the atomic-scale near-field confinement in a single plasmonic nanoparticle, constituted here by a Na_{380} cluster. The polarizability of the Na_{380} cluster obtained with the atomistic simulations shows a well-defined plasmonic peak near 3.35 eV, associated with a typical dipolar excitation along the axis of the external driving field. Further technical details of the calculation are addressed in the Supporting Information.

Figure 1 shows the local near-field distribution around the Na_{380} cluster for different polarizations of the incident field of amplitude E_0, both at the dipolar plasmonic resonance energy (panels a–c) and out of resonance (panels d–f). The orientation of the cluster relative to the external field is further clarified in Figure S1 in the Supporting Information. We show the data in the (y, z) plane passing through the center of the cluster for two different incident linear polarizations (along y axis in panel a and along z axis in panel b). As observed in the plots, when the atomistic structure is accounted for, the near fields dramatically depend on the cluster orientation with respect to the polarization direction. Even if the general dipolar pattern of the induced fields is preserved, the underlying icosahedral geometry of the atomic arrangement can be clearly recognized. Most importantly, we can clearly identify subnanometric "hot-spots" characterized by strongly localized fields at the metal-vacuum interface. The enhancement at these "hot-spots" is not dramatically larger than that of the overall background of the plasmon-enhanced near fields, but it carries a very distinctive localization with it. The "hot-spots" of the Na_{380} cluster in panels a and b are related to the atomic-scale vertices and edges of the icosahedron cluster structure. Obviously, a quantum (or classical) calculation that considers smooth surfaces and thus ignores the atomistic nature of the particles cannot address these subnanometric features in the near fields, and misses the description of atomic-scale field localization. This is illustrated in panel c where the results based on the JM for the perfectly spherical cluster are shown for comparison. In this case, the induced fields are independent of the cluster orientation with respect to the incident field and feature the

DOI: 10.1021/acs.nanolett.5b00759
Nano Lett. 2015, 15, 3410−3419

typical smooth dipolar pattern of the plasmon induced along the polarization direction (y-axis chosen here). While outside the cluster the TDDFT-JM description is very similar to the classical Mie[88] results for a metal sphere described with a Drude dielectric function, quantum effects are apparent inside the cluster where the screening of fields is accompanied by Friedel-like oscillations.[89]

Remarkably, in the atomistic results we observe an atomic-scale lightning rod effect[65] that can be related to the macroscopic lightning rod effect[66,90] resulting from the classical field divergence at infinitely sharp tips. The atomistic structure of the material naturally sets a quantum constraint to the notion of "infinitely sharp" since, obviously, an effective curvature radius cannot be smaller than that given by the electron density profile of the single atom. The local dipoles responsible for the subnanometric field confinement are formed by the collective response of the protruding groups of atoms screened by the rest of the cluster. Therefore, at resonance excitation conditions, the near field structure of the cluster, as obtained from our atomistic calculations, can be understood as a combination of two effects: (i) the overall plasmonic near-field enhancement at the dipolar mode, and (ii) the atomic scale lightning rod effect which arises because of the presence of vertices and edges between the atomic planes forming the cluster surface, and allowing to further focus the energy into an extremely small area. We can thus establish an analogy with the macroscopic self-similar plasmonic nanoantennas, where larger antennas produce further enhancement on the smallest ones, like in a plasmonic lens.[91−93] Here, the subnanometer "hot-spots" induced around atomically sharp features are fed in a cascade fashion by the plasmonic field of the larger and smoother nanometric plasmonic system (hosting particle or dimer).

The lightning rod effect can be isolated in the absence of a plasmonic resonance. We illustrate this in Figure 1d−f where we plot the near-field distribution around the Na_{380} cluster, obtained for incident plane wave irradiation off resonance with the plasmonic dipolar mode. Except for this change of wavelength, we used the same conditions regarding polarization, geometry, and atomistic or jellium modeling of the cluster, as in panels a−c. In the off-resonance situation, the atomic-scale "hot-spots" are still present for the Na_{380} cluster for both polarizations, providing a substantial local enhancement that extends a few angstroms from the cluster surface. In this case, the lightning rod effect is isolated from the plasmonic effect, even though overall, in the absence of the resonant dipolar plasmon mode, the induced near fields are several times weaker, which also holds for the "hot-spots" regions.

We emphasize next the importance of atomic-scale features in a canonical structure in plasmonics, the metallic nanogap. By placing two metallic nanoparticles together, we can create a plasmonic nanogap where the coupling of plasmonic modes generates new hybridized solutions that are red-shifted with respect to the original resonances of the individual particles.[3,94] In Figure 2 we analyze the importance of the atomistic details of the nanogap by selecting results obtained for three main configurations that present different terminations of the interfaces at the gap: (i) facet-to-facet, (ii) tip-to-facet, and (iii) tip-to-tip. For completeness, we also consider the case of a dimer formed by two jellium spheres, thus forming a nanogap bound by smooth surfaces. The spectral behavior of the nanogap resonances as a function of the interparticle separation distance, d_{sep}, is displayed in Figure 2a−d, where we plot the absorption cross-section, σ_{abs}, for each case: (a) facet-to-facet, (b) tip-to-facet, (c) tip-to-tip, and (d) jellium. The polarization of the incident field is set along the dimer axis.

The corresponding atomistic structure of the different nanogap models can be found in Figure 2e−g, along with the distribution of the induced near-field for an interparticle distance of 10 Å, evaluated at the BDP resonance frequency for each type of gap. In the case of the atomistic calculations, the separation distance, d_{sep}, is measured between the closest atoms across the gap. Separation distances smaller than 1 Å, as well as negative distances (corresponding to the case of overlapping clusters[3]), have been modeled using modified structures in which atomic layers are successively removed from one of the clusters (areas marked with A, B, and C at the bottom of panels a−c). More information on the actual structures can be found in the Supporting Information. For a consistent comparison, in the jellium case we also consider the separation distance as defined from the surface atomic layers rather than from the jellium edges.

In Figures 2a−d we can distinguish clearly the evolution of the hybridized bonding dimer plasmon (BDP) for each gap configuration: the BDP redshifs as the separation distance between the nanoparticles decreases.[3,28,29] Consistent with previous descriptions, this trend holds down to separations of the order of a few angstroms. When the particles are even closer together, the system enters a new regime due to the emergence of the tunneling current across the gap at optical frequencies.[62,63,95] In the quantum tunneling regime, the BDP is progressively screened, and it disappears from the spectrum. For increasing current across the gap, charge-transfer plasmons (CTPs)[96] that correspond to the polarization of the entire dimer with interparticle charge transfer, emerge. Despite the common general trends for the three atomistic calculations, remarkable differences arise with regard to the exact separation distance where the quantum effects occur. For the same separation distance d_{sep}, in the facet-to-facet configuration the tunneling current is larger because of the larger contact area. Thus, the BDP disappears and the CTP emerges at the largest separation distances, (6 and 4 Å, respectively). In the configurations characterized by the presence of a tip, the tunneling current is confined mainly to the area around the tip, thus the overall tunneling current is smaller. As a consequence, smaller separation distances, d_{sep}, are required for the quenching of the BDP and appearance of the CTPs in such cases, as clearly observed in Figure 2b and c.

We now explore the influence of the different atomistic configurations of the plasmonic gap on the near-field distribution at the resonance position. In Figure 2e−h the induced near-fields are shown in the (y, z) plane of the dimer passing through the centers of the nanoparticles for the facet-to-facet (e), tip-to-facet (f), tip-to-tip (g), and jellium spherical (h) configurations. The width of the gap is set in all the cases to d_{sep} = 10 Å, with incident light in resonance with the hybridized BDP corresponding to the position marked with a green dot on the spectra to the left. The Coulomb coupling between induced charges of opposite signs across the gap leads to a strong localization and enhancement of the near fields in the gap. This effect is widely exploited in surface-enhanced spectroscopies and microscopies. Overall, the nanometric near-field distributions obtained in the full atomistic calculations at the BDP frequency show similar gross features to those in the JM calculations. However, the exact atomistic structure of the junction determines the details of the near-field distribution,

DOI: 10.1021/acs.nanolett.5b00759
Nano Lett. 2015, 15, 3410−3419

and in particular the appearance of the extremely localized "hot spots". As observed in Figure 2e, the gap characterized by a facet-to-facet configuration features a well-defined and homogeneous field enhancement that extends over the entire gap, as expected from a scaled parallel plate capacitor. The lateral localization of the hot-spot between the particles is thus determined by the corresponding nanometric facet size. Albeit much less intense, atomic-scale hot spots can be also identified at the edges and vertices of the different facets of the nanocrystal surfaces, both near and opposite to the plasmonic gap. These are due to the atomic-scale lightning rod effect, similar to that found in Figure 1 for the single particle. Compared to the JM with a perfectly spherical geometry, atomic-scale features at the cluster facets increase the Landau damping of the BDP and thus broaden the plasmon resonance peaks (see Supporting Information).

A remarkable situation is achieved when exploiting the atomic-scale lightning rod effect in a tip-to-facet or in a tip-to-tip configurations in the gap (Figure 2f and g). In such situations, the tip-induced enhancement is superimposed on the already intense background field of the plasmonic resonance, producing a further increase of the value of the enhancement, and more importantly, an extreme localization of this local near-field down to an extension of a few angstroms. This extreme confinement of the fields is missed in the JM model that assumes a smooth density profile, as shown in Figure 2h. By means of our realistic atomistic calculations, we have thus shown that atomic-scale hot spots are possible, and they may be relevant to allow superresolution in a variety of experimental near-field techniques.[49,70,71]

To analyze the field enhancement induced at each of the plasmonic cavities quantitatively, we show in Figure 3 the maximum induced near-field enhancement at resonance in the middle of the gap, $|\mathbf{E}_{ind}^{max}|/\mathbf{E}_0$ (panel a), and the effective localization area of the near-field, $\mathcal{A}$ (panel b), as a function of the gap separation d_{sep}. We have chosen to plot and analyze the field distributions at those resonance energies that produce the largest maximum of the induced near-field at each configuration. Thus, for the tip-to-facet and tip-to-tip gaps we follow the BDP-QP mode around 3 eV, whereas for the facet-to-facet configuration data, for $d_{sep} \leq 5$ Å, we follow the CTP mode appearing at lower energies. The local near-fields are obtained for the same configurations and light incidence as in Figure 2. The maximum enhancement is found in all the cases for $d_{sep} \approx 7$ Å (see Figure 3a). As discussed in detail in the Supporting Information, when the gap size is reduced below this value, the electron tunneling neutralizes the plasmon-induced charges at the metal surfaces across the gap, and reduces the induced fields.[62,63] For larger separations, the coupling between the plasmons of the individual particles becomes smaller thus the field enhancement progressively decreases, and the differences due to the atomic-scale features are also attenuated. When atomic-scale tip(s) is (are) present in the junction, the maximum near-field enhancement is about 1.5 times larger than that of a facet-to-facet configuration (red and blue lines vs green line in Figure 3a), emphasizing the importance of the fine details of the gap.

Together with the absolute value of the field enhancement, the confinement is an aspect of particular interest in nanophotonics. In Figure 3b, we plot the effective localization area, $\mathcal{A}$, of the BDP for each atomistic configuration. $\mathcal{A}$ is defined according to the following expression:

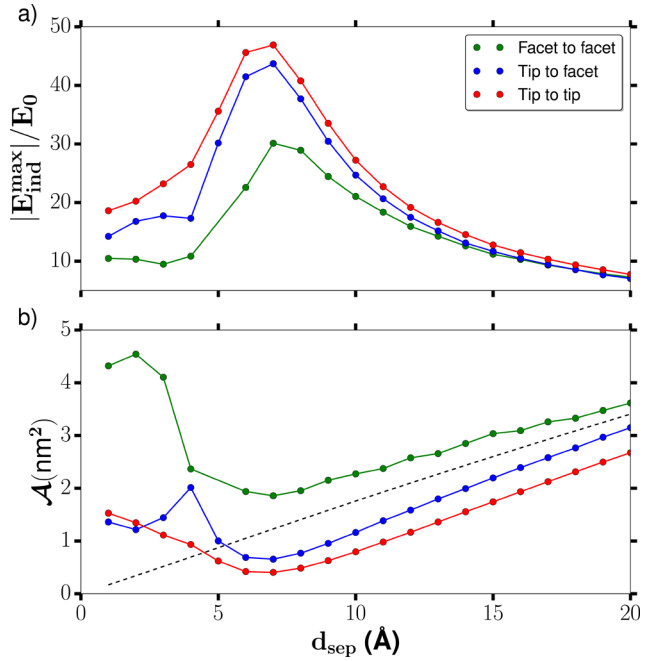

Figure 3. (a) TDDFT calculation of the maximum enhancement of the local induced-field $|\mathbf{E}_{ind}^{max}|/\mathbf{E}_0$ at the center of a gap between two particles showing different atomistic configurations, as a function of the separation between the particles forming the gap, d_{sep}. The separation is defined as the distance between the most protruding atoms in both clusters. The green line stands for the facet-to-facet configuration in the gap, the blue line stands for the tip-to-facet configuration and the red line stands for the tip-to-tip configuration. (b) Effective localization area $\mathcal{A}$ of the local field in the midplane of the gap as defined in the text (eq 1) for each of the three configurations. As a reference, the localization of the BDP for a pair of spherical particles given by a classical calculation is displayed as a dashed line. The plotted data correspond to the resonance energies that produce the largest maximum of the induced near-field for each configuration and distance. For the facet-to-facet case this corresponds to the CTP mode for d_{sep} <5 Å. For the tip-to-facet and tip-to-tip gaps we follow the BDP and QP modes around 3 eV. The different dependence of $\mathcal{A}$ on d_{sep} for the BDP and QP modes is clearly visible in the singular behavior of the $\mathcal{A}$ data around 4 Å for the tip-to-facet case, which is almost undetectable in the more gradual BDP-QP transition of the tip-to-tip gap.

$$\mathcal{A} = \frac{1}{h}\int_V \frac{|\mathbf{E}_{ind}(x,y,z)|^2}{|\mathbf{E}_{ind}^{max}|^2}\mathrm{d}V \qquad (1)$$

where $|\mathbf{E}_{ind}(x,y,z)|$ is the modulus of the induced field in a thin slab of volume V and thickness h = 0.63 Å along z direction, centered in the middle of the gap. $|\mathbf{E}_{ind}^{max}|$ is the maximum value of the field in the integration volume. Therefore, $\mathcal{A}$ provides a measure of the effective area in which the induced field is localized in the (x,y) plane in the middle of the gap. The results are plotted in Figure 3b as a function of separation distance, for the same excitation wavelengths used in Figure 3a. As expected, the three different atomistic configurations show maximum localization of the BDP mode at separations of about 7 Ångstroms, corresponding to the separation of maximal enhancement described above. For smaller separation distances, when the tunneling current is established, the field is expelled out from the gap and thus becomes less localized.[49] The tip-to-tip morphology, for which the lightning rod effect is more pronounced, provides the strongest localization among all. The

DOI: 10.1021/acs.nanolett.5b00759
Nano Lett. 2015, 15, 3410−3419

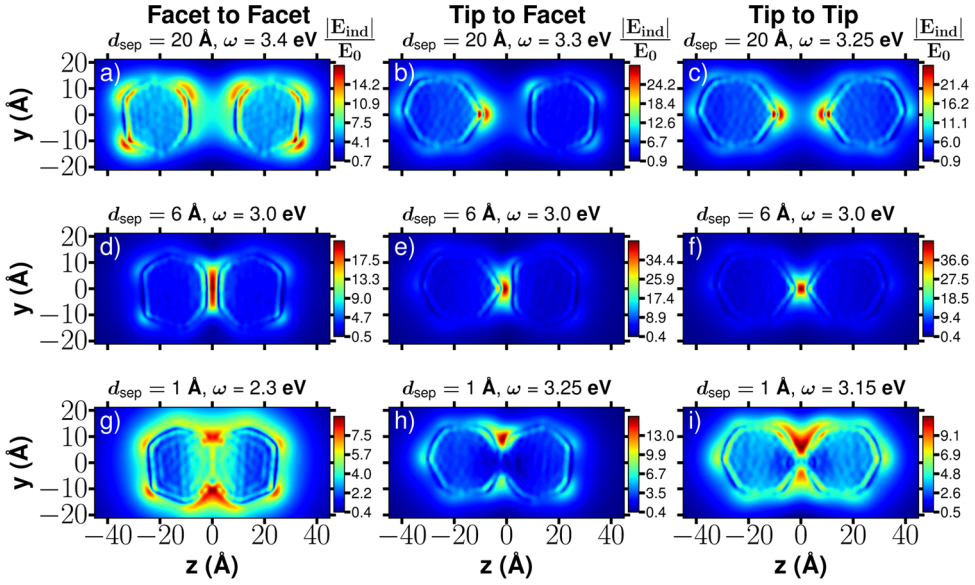

Figure 4. Local induced-field enhancement in the (y,z) plane that contains the axis of a Na metallic dimer for the case of a facet-to-facet configuration at the gap (left column), tip-to-facet configuration (middle column), and tip-to-tip configuration (right column). The incident plane wave is polarized along the dimer axis. From top to bottom, three cases of decreasing separation distance are shown for each configuration: d_{sep} = 20 Å (top row, a–c), d_{sep} = 6 Å (middle row, d–f), and d_{sep} = 1 Å (bottom row, g–i). The field is always plotted at the frequency of the most intense resonance in the absorption cross-section of the dimer. This corresponds to the BDP mode in most cases, except for the facet-to-facet case at the closest separation, that corresponds to the CTP mode (panel g).

minimum $\mathcal{A}$ in this case is 0.4 nm^2, clearly indicating that the plasmonic fields can be localized down to lateral dimensions of a few thousandths of the incident wavelength with the help of an atomic feature. This value of $\mathcal{A}$ is up to 4 times smaller than that for the facet-to-facet configuration, for the same d_{sep} = 7 Å.

For reference purposes, we also plot in Figure 3b, as a black dashed line, the localization corresponding to a classical calculation of the BDP in a gap formed by spherical particles of the same size, and characterized by a Drude-like response that corresponds to the same electronic density as in the atomistic calculations. As observed in the figure, the localization in this case tends linearly to zero for small d_{sep}. This unphysical result is due to the lack of dynamical screening and tunneling in the classical description. It is interesting to note that all the systems show a linear dependence of the localization with separation distance, as the gap is opening. This is a reminiscence of the two effects involved: the overall plasmonic effect, plus the atomistic effect. The classical estimation in spherical particles indeed establishes a reference for the behavior of the localization at the different atomistic gaps: when an atomic-scale tip is present in the gap, the linear dependency is pushed below this classical result (larger slope of red and blue lines). However, for the case of a facet-to-facet gap, the linear dependency shows a smaller slope, setting values of the localization area that exceed those of the confinement by classical spherical surfaces. In this case the minimal localization area of the field is approximately given by the surface of the facet, as one would expect for a flat capacitor. Therefore, our classical result for the induced-field localization establishes a good benchmark to distinguish between subplasmonic and plasmonic localization, depending on whether the linear tendencies show a more or less pronounced change, respectively, compared to the classical reference of spherical particles.

As a further remark, it should be noted that the presence of subnanometric "hot spots" may only weakly affect $\mathcal{A}$, as defined by eq 1, in large plasmonic systems because the integral will be dominated by the overall plasmonic field structure in the gap. This is actually one of the reasons why plasmonic enhancement is a robust and reliable tool in many standard field-enhanced spectroscopies. Nonetheless, such local behavior at the atomic scale could be important to determine the precise properties of the near field at particular positions, probed, for example, by molecular targets[69,72] or by electron emission,[97] which are extremely sensitive to these spatial inhomogeneities independently of how large the plasmonic background is.

The quantitative analysis of the evolution of the near fields with the gap size performed in Figure 3 is further illustrated in Figure 4 and Figure 5 which allow for a more intuitive insight into the role of the atomistic structure on the localization. In Figure 4, we plot the distribution of induced near fields in the (y, z) plane containing the centers of the nanoparticles. The results are shown for the facet-to-facet (left column), tip-to-facet (middle column), and tip-to-tip (right column) configurations of the nanogap. Three separations, d_{sep} = 20 Å (top row), d_{sep} = 6 Å (middle row), and d_{sep} = 1 Å (bottom row), are chosen here to represent respectively weak interaction, strong interaction, and strong tunneling regimes. For the largest separation, d_{sep} = 20 Å, the coupling between nanoparticles is weak, therefore the near fields around each nanoparticle of the dimer resemble those of the individual particles, as presented in Figure 1. Nevertheless, stronger fields at the facing surfaces across the gap can be clearly observed, indicating the onset of the hybridization of the BDP.

Atomic-scale "hot-spots" are visible all over the nanoparticle surface, particularly in regions associated with atomic edges at the contact of the crystalline facets. These "hot-spots" are apparent for the flat-facet gap (top row, left), but are even more pronounced in the presence of a tip-like geometry pointing toward the junction, and aligned with the polarization direction (middle and right). As the particles get closer, d_{sep} = 6 Å (middle row), the field enhancement at the gap becomes very

DOI: 10.1021/acs.nanolett.5b00759
Nano Lett. 2015, 15, 3410–3419

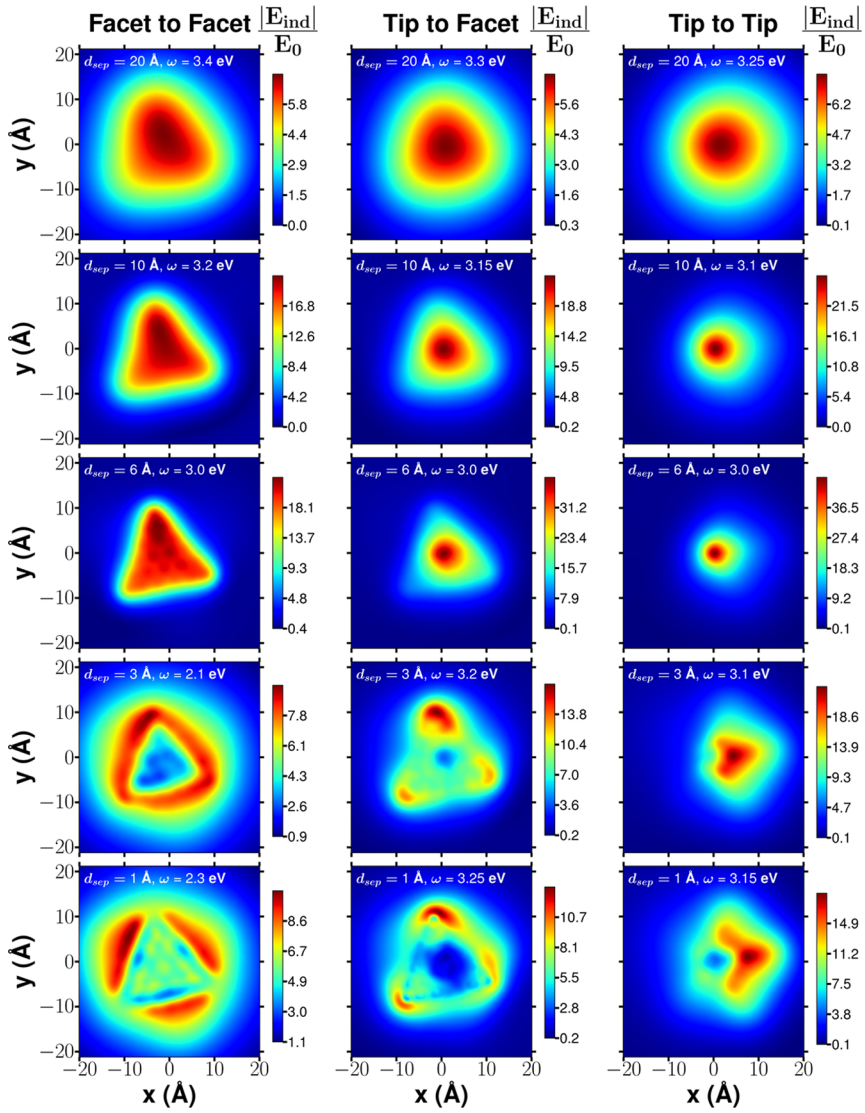

Figure 5. Local induced-field enhancement at resonance in the midplane of the gap between two Na_{380} clusters for our three configurations, facet-to-facet gap (left column), tip-to-facet (middle column) and tip-to-tip (right column). The incident planewave is *z*-polarized.From top to bottom each case shows a decreasing separation distance for each configuration, from d_{sep} = 20 Å (largely separated particles, on the top row) to d_{sep} = 1 Å (interpenetrating situation on the bottom row). The influence of the atomic scale features at the nanogaps is directly noticeable.

intense (notice the absolute value of the corresponding scales). For the facet-to-facet situation (middle row, left column) the enhancement is homogeneous inside the gap as a consequence of the flat-surface capacitor geometry. In contrast, when a tip-like configuration is present in the gap, it leads to a particularly strong field enhancement and to clear subnanometer localization at the center of the gap, consistent with the results of Figure 3. For very small separation distances (bottom row), the electronic densities of the two particles strongly overlap, essentially producing a nanometric neck of continuous electron density. Therefore, the region of enhanced field is expelled to the edges of the junction.[95,96] This is accompanied by an overall weakening of the fields in the junction region, which eventually become comparable in intensity to the hot spots at other locations of the dimer surfaces.

The evolution of the field confinement in the gap as a function of separation distance, d_{sep}, and the corresponding change of the localization area $\mathcal{A}$ is illustrated in Figure 5, where the field enhancement is shown in the (x, y) midplane between the two particles for each configuration (facet-to-facet on the left column, tip-to-facet on the middle column, and tip-to-tip on the right column). When the particles are far away from each other (d_{sep} = 20 Å), a relatively broad spatial profile of the plasmonic near-field is obtained (top row). This profile is mainly determined by low order multipoles at each nanoparticle so that the features due to the specific atomistic structures of the nanoparticle surfaces are weak. For smaller separation, d_{sep} = 10 Å, the profile of the near fields reflects the atomistic structure of the nanoparticle surfaces across the gap, showing a triangular shape for the facet-to-facet configuration, a round spot for the tip-to-tip configuration, and a round spot on top of a triangular background for the tip-to-facet configuration. As expected from the results in Figure 3, the tip-to-tip configuration corresponds to the strongest field confinement with the smallest spot size reduced to atomic dimensions, i.e., below 1 nm^2 for $d_{sep} \approx 6$ Å. For the parallel capacitor facet-to-facet configuration, the spot profile and size change only slightly when d_{sep} is reduced from 10 to 6 Å, and the tip-to-facet configuration features the intermediate situation (see also Figure 4). We thus show here that the widely accepted picture

DOI: 10.1021/acs.nanolett.5b00759
Nano Lett. 2015, 15, 3410−3419

of the overall reduction of the localization area $\mathcal{A}$ for smaller d_{sep}, as obtained from previous studies for smooth particles,[62,95,98] has to be taken with caution, as it can be altered by the atomistic structure of the gap. For d_{sep} below 6 Å (lower rows), the tunneling current expels the fields from the middle of the gap. This effect is particularly nicely observed for the CTP mode in the facet-to-facet configuration.

In conclusion, by means of first-principles full-atomistic TDDFT calculations, we have demonstrated that the distribution of the near-field close to plasmonic nanoparticles presents subnanometric hot spots that reflect atomic-scale features at the nanoparticle surface. In our case, these features consist of vertices and edges at the contact of the crystallographic facets of the particles. In particular, for the plasmonic dimer, we have shown that the field localization and enhancement inside the plasmonic nanogaps can be very different depending on whether the distribution of the atoms at the gap defines a flat surface, or presents atomic-scale tip-like protrusions. We obtain that the far field also depends on the atomic configuration but in a less marked fashion as expected.

Our findings provide new insights into the limits of plasmonic localization. The presence of atomic-size features, e.g., formed by edges and vertices between crystalline facets in a nanoparticle, gives rise to near fields localized in regions with linear dimensions of a few angstroms, i.e., literally of atomic size. This effect can be related to the classical divergence of a field due to the presence of sharp edges. Indeed, the vertex ending by a single atom, as the one considered here, would be the example of the sharpest possible tip. Furthermore, the fields enhanced at the atomic-scale hot spots are intensified by the presence of the overall plasmonic background enhancement, following a cascade effect. Based on this parallelism, we can establish an atomic-scale analogy with the macroscopic plasmonic lens of self-similar antennas.[91−93,99]

As demonstrated here, in a realistic nanogap, the key features of the field enhancement can easily reach the atomic scale. Therefore, a description of the plasmonic response based on smooth interface profiles, either classical or quantum, might not be able to address this atomic-scale near-field regime. To understand and optimize certain experimental situations operating in the subnanometer-scale, it might be mandatory to develop computational schemes that account for the atomistic structural details. Such sensitivity to the atomic details of a structure could explain the lack of reproducibility between apparently similar experiments,[100] but could also provide a root for further optimization of morphologies. The resolution in optics depends on atomic-scale features at the nanoparticle(s) surface, a remarkable finding that might provide new insights into the limits of plasmon localization, and has important consequences for the limits of optical resolution in field-enhanced spectroscopies[101,102] and microscopies.[49,70,71]

■ ASSOCIATED CONTENT

Supporting Information

Additional details on the computational parameters used in our calculations, and how they influence the results, on the structures of the different systems studied here, as well as a more detailed discussion of the data regarding the optical absorption versus d_{sep} in Figure 2, together with the study of the corresponding currents established across the gap. The Supporting Information is available free of charge on the ACS Publications website at DOI: 10.1021/acs.nanolett.5b00759.

■ AUTHOR INFORMATION

Corresponding Authors

*E-mail: aizpurua@ehu.es.
*E-mail: sqbsapod@ehu.es.

Notes

The authors declare no competing financial interest.

■ ACKNOWLEDGMENTS

We acknowledge useful discussions with Jeremy Baumberg and Volker Deckert regarding practical optical resolution issues in field-enhanced spectroscopy and microscopy, and Dietrich Foerster regarding efficient TDDFT calculations. We acknowledge financial support from projects FIS2013-14481-P and MAT2013-46593-C6-2-P from MINECO. M.B., P.K., F.M., and D.S.P. also acknowledge support from the ANR-ORGAVOLT project and the Eurorègion Aquitaine-Euskadi program. M.B. acknowledges support from the Departamento de Educación of the Basque Government through a PhD grant, as well as from Euskampus and the DIPC at the initial stages of this work. R.E. and P.K. acknowledge financial support from the Fellows Gipuzkoa program of the Gipuzkoako Foru Aldundia through the FEDER funding scheme of the European Union, "Una manera de hacer Europa".

■ REFERENCES

(1) Oldenburg, S. J.; Averitt, R. D.; Westcott, S. L.; Halas, N. J. *Chem. Phys. Lett.* **1998**, *288*, 243−247.
(2) Xu, H.; Bjerneld, E. J.; Käll, M.; Börjesson, L. *Phys. Rev. Lett.* **1999**, *83*, 4357−4360.
(3) Romero, I.; Aizpurua, J.; Bryant, G. W.; García de Abajo, F. J. *Opt. Express* **2006**, *14*, 9988−9999.
(4) Willets, K. A.; van Duyne, R. P. *Annu. Rev. Phys. Chem.* **2007**, *58*, 267−297.
(5) Pelton, M.; Aizpurua, J.; Bryant, G. *Laser Photonics Rev.* **2008**, *2*, 136−159.
(6) Alvarez-Puebla, R.; Liz-Marzán, L. M.; García de Abajo, F. J. *J. Phys. Chem. Lett.* **2010**, *1*, 2428−2434.
(7) Moskovits, M. *Rev. Mod. Phys.* **1985**, *57*, 783−826.
(8) Nie, S.; Emory, S. R. *Science* **1997**, *275*, 1102−1106.
(9) Neubrech, F.; Pucci, A.; Cornelius, T.; Karim, S.; García-Etxarri, A.; Aizpurua, J. *Phys. Rev. Lett.* **2008**, *101*, 157403.
(10) Le Ru, E. C.; Etchegoin, P. G. *Annu. Rev. Phys. Chem.* **2012**, *63*, 65−87.
(11) Atwater, H. A.; Polman, A. *Nat. Mater.* **2010**, *9*, 205−213.
(12) Linic, S.; Christopher, P.; Ingram, D. B. *Nat. Mater.* **2011**, *10*, 911−921.
(13) MacDonald, K. F.; Sámson, Z. L.; Stockman, M. I.; Zheludev, N. I. *Nat. Photonics* **2008**, *3*, 55−58.
(14) Large, N.; Abb, M.; Aizpurua, J.; Muskens, O. L. *Nano Lett.* **2010**, *10*, 1741−1746.
(15) Berrier, A.; Ulbricht, R.; Bonn, M.; Rivas, J. G. *Opt. Express* **2010**, *18*, 23226−23235.
(16) Chen, J.; Badioli, M.; Alonso-González, P.; Thongrattanasiri, S.; Huth, F.; Osmond, J.; Spasenović, M.; Centeno, A.; Pesquera, A.; Godignon, P.; Zurutuza Elorza, A.; Camara, N.; García de Abajo, F. J.; Hillenbrand, R.; Koppens, F. H. L. *Nature* **2012**, *487*, 77−81.
(17) Lal, S.; Clare, S. E.; Halas, N. J. *Acc. Chem. Res.* **2008**, *41*, 1842−1851.
(18) Link, S.; El-Sayed, M. A. *J. Phys. Chem. B* **1999**, *103*, 8410−8426.
(19) Jin, R.; Cao, Y.; Mirkin, C. A.; Kelly, K. L.; Schatz, G. C.; Zheng, J. G. *Science* **2001**, *294*, 1901−1903.
(20) Averitt, R.; Sarkar, D.; Halas, N. *Phys. Rev. Lett.* **1997**, *78*, 4217−4220.
(21) Aizpurua, J.; Hanarp, P.; Sutherland, D.; Kall, M.; Bryant, G. W.; García de Abajo, F. J. *Phys. Rev. Lett.* **2003**, *90*, 057401.

DOI: 10.1021/acs.nanolett.5b00759
Nano Lett. 2015, 15, 3410−3419

(22) Aizpurua, J.; Bryant, G. W.; Richter, L. J.; García de Abajo, F. J.; Kelley, B. K.; Mallouk, T. *Phys. Rev. B* **2005**, *71*, 235420.
(23) Novotny, L. *Phys. Rev. Lett.* **2007**, *98*, 266802.
(24) Dorfmüller, J.; Vogelgesang, R.; Weitz, R. T.; Rockstuhl, C.; Etrich, C.; Pertsch, T.; Lederer, F.; Kern, K. *Nano Lett.* **2009**, *9*, 2372−2377.
(25) Funston, A. M.; Novo, C.; Davis, T. J.; Mulvaney, P. *Nano Lett.* **2009**, *9*, 1651−1658.
(26) Hao, F.; Nehl, C. L.; Hafner, J. H.; Nordlander, P. *Nano Lett.* **2007**, *7*, 729−732.
(27) Novikov, S. M.; Sánchez-Iglesias, A.; Schmidt, M. K.; Chuvilin, A.; Aizpurua, J.; Grzelczak, M.; Liz-Marzán, L. M. *Part. Part. Syst. Charact.* **2014**, *31*, 77−80.
(28) Su, K.-H.; Wei, Q.-H.; Zhang, X.; Mock, J. J.; Smith, D. R.; Schultz, S. *Nano Lett.* **2003**, *3*, 1087−1090.
(29) Rechberger, W.; Hohenau, A.; Leitner, A.; Krenn, J. R.; Lamprecht, B.; Aussenegg, F. R. *Opt. Commun.* **2003**, *220*, 137−141.
(30) Fan, J. A.; Wu, C.; Bao, K.; Bao, J.; Bardhan, R.; Halas, N. J.; Manoharan, V. N.; Nordlander, P.; Shvets, G.; Capasso, F. *Science* **2010**, *328*, 1135−1138.
(31) Hentschel, M.; Saliba, M.; Vogelgesang, R.; Giessen, H.; Alivisatos, A. P.; Liu, N. *Nano Lett.* **2010**, *10*, 2721−2726.
(32) Kelly, K. L.; Coronado, E.; Zhao, L. L.; Schatz, G. C. J. *Phys. Chem. B* **2003**, *107*, 668−677.
(33) Schnell, M.; García-Etxarri, A.; Huber, A. J.; Crozier, K.; Aizpurua, J.; Hillenbrand, R. *Nat. Photonics* **2009**, *3*, 287−291.
(34) Halas, N. J.; Lal, S.; Chang, W.-S.; Link, S.; Nordlander, P. *Chem. Rev.* **2011**, *111*, 3913−3961.
(35) Mühlschlegel, P.; Eisler, H.-J.; Martin, O. J. F.; Hecht, B.; Pohl, D. W. *Science* **2005**, *308*, 1607−1609.
(36) Novotny, L.; van Hulst, N. *Nat. Photonics* **2011**, *5*, 83−90.
(37) Kern, J.; Großmann, S.; Tarakina, N. V.; Häckel, T.; Emmerling, M.; Kamp, M.; Huang, J.-S.; Biagioni, P.; Prangsma, J. C.; Hecht, B. *Nano Lett.* **2012**, *12*, 5504−5509.
(38) Ward, D. R.; Hüser, F.; Pauly, F.; Cuevas, J. C.; Natelson, D. *Nat. Nanotechnol.* **2010**, *5*, 732−736.
(39) Sigle, D. O.; Mertens, J.; Herrmann, L. O.; Bowman, R. W.; Ithurria, S.; Dubertret, B.; Shi, Y.; Yang, H. Y.; Tserkezis, C.; Aizpurua, J.; Baumberg, J. J. *ACS Nano* **2015**, *9*, 825−830.
(40) Danckwerts, M.; Novotny, L. *Phys. Rev. Lett.* **2007**, *98*, 026104.
(41) Grillet, N.; Manchon, D.; Bertorelle, F.; Bonnet, C.; Broyer, M.; Cottancin, E.; Lermé, J.; Hillenkamp, M.; Pellarin, M. *ACS Nano* **2011**, *5*, 9450−9462.
(42) Sun, M.; Xu, H. *Small* **2012**, *8*, 2777−2786.
(43) Christopher, P.; Xin, H.; Marimuthu, A.; Linic, S. *Nat. Mater.* **2012**, *11*, 1044−1050.
(44) Mukherjee, S.; Libisch, F.; Large, N.; Neumann, O.; Brown, L. V.; Cheng, J.; Lassiter, J. B.; Carter, E. A.; Nordlander, P.; Halas, N. J. *Nano Lett.* **2013**, *13*, 240−247.
(45) Baffou, G.; Quidant, R. *Chem. Soc. Rev.* **2014**, *43*, 3898−3907.
(46) Kneipp, K.; Wang, Y.; Kneipp, H.; Perelman, L.; Itzkan, I.; Dasari, R.; Feld, M. *Phys. Rev. Lett.* **1997**, *78*, 1667−1670.
(47) Kühn, S.; Håkanson, U.; Rogobete, L.; Sandoghdar, V. *Phys. Rev. Lett.* **2006**, *97*, 017402.
(48) Anger, P.; Bharadwaj, P.; Novotny, L. *Phys. Rev. Lett.* **2006**, *96*, 113002.
(49) Zhang, R.; Zhang, Y.; Dong, Z. C.; Jiang, S.; Zhang, C.; Chen, L. G.; Zhang, L.; Liao, Y.; Aizpurua, J.; Luo, Y.; Yang, J. L.; Hou, J. G. *Nature* **2013**, *498*, 82−86.
(50) Ozbay, E. *Science* **2006**, *311*, 189−193.
(51) Huang, J.-S.; Feichtner, T.; Biagioni, P.; Hecht, B. *Nano Lett.* **2009**, *9*, 1897−1902.
(52) Prangsma, J. C.; Kern, J.; Knapp, A. G.; Grossmann, S.; Emmerling, M.; Kamp, M.; Hecht, B. *Nano Lett.* **2012**, *12*, 3915−3919.
(53) Stolz, A.; Berthelot, J.; Mennemanteuil, M.-M.; Colas des Francs, G.; Markey, L.; Meunier, V.; Bouhelier, A. *Nano Lett.* **2014**, *14*, 2330−2338.
(54) Runge, E.; Grosss, E. K. U. *Phys. Rev. Lett.* **1984**, *52*, 997−1000.
(55) Parr, R. G.; Weitao, Y. *Density-functional theory of atoms and molecules*; Oxford University Press: Oxford, 1989.
(56) Feibelman, P. J. *Phys. Rev. B* **1975**, *12*, 1319−1336.
(57) Liebsch, A.; Schaich, W. L. *Phys. Rev. B* **1995**, *52*, 14219−14234.
(58) Teperik, T. V.; Nordlander, P.; Aizpurua, J.; Borisov, A. G. *Phys. Rev. Lett.* **2013**, *110*, 263901.
(59) Monreal, R. C.; Antosiewicz, T. J.; Apell, S. *New J. Phys.* **2013**, *15*, 083044.
(60) Negre, C. F. A.; Perassi, E. M.; Coronado, E. A.; Sánchez, C. G. *J. Phys.: Condens. Matter* **2013**, *25*, 125304.
(61) Iida, K.; Noda, M.; Ishimura, K.; Nobusada, K. *J. Phys. Chem. A* **2014**, *118*, 11317−11322.
(62) Zuloaga, J.; Prodan, E.; Nordlander, P. *Nano Lett.* **2009**, *9*, 887−891.
(63) Marinica, D. C.; Kazansky, A. K.; Nordlander, P.; Aizpurua, J.; Borisov, A. G. *Nano Lett.* **2012**, *12*, 1333−1339.
(64) Zhang, P.; Feist, J.; Rubio, A.; García-González, P.; García-Vidal, F. J. *Phys. Rev. B* **2014**, *90*, 161407.
(65) Gersten, J.; Nitzan, A. *J. Chem. Phys.* **1980**, *73*, 3023−3037.
(66) Novotny, L.; Bian, R.; Xie, X. *Phys. Rev. Lett.* **1997**, *79*, 645−648.
(67) Le, F.; Brandl, D. W.; Urzhumov, Y. A.; Wang, H.; Kundu, J.; Halas, N. J.; Aizpurua, J.; Nordlander, P. *ACS Nano* **2008**, *2*, 707−718.
(68) Zuloaga, J.; Prodan, E.; Nordlander, P. *ACS Nano* **2010**, *4*, 5269−5276.
(69) Payton, J. L.; Morton, S. M.; E, M. J.; Jensen, L. *J. Chem. Phys.* **2012**, *136*, 214103.
(70) Yano, T.-a.; Ichimura, T.; Kuwahara, S.; HDhili, F.; Uetsuki, K.; Okuno, Y.; Verma, P.; Kawata, S. *Nat. Commun.* **2013**, *4*, 2592.
(71) Deckert-Gaudig, T.; Deckert, V. *Small* **2009**, *16*, 432−436.
(72) Payton, J. L.; Morton, S. M.; E, M. J.; Jensen, L. *Acc. Chem. Res.* **2014**, *47*, 88−99.
(73) Vang, R. T.; Honkala, K.; Dhal, S.; Vestergaard, E. K.; Schandt, J.; Laegsgaard, E.; Clausen, B. S.; Norskov, J. K.; Besenbacher, F. *Nature* **2005**, *4*, 160−162.
(74) Woodruff, D. P., Ed. *Atomic clusters: From Gas Phase to Deposited*; The Chemical Physics of Solid Surfaces, 12; Elsevier Science: Amsterdam, 2007.
(75) Heiz, U., Landman, U., Eds. *Nanocatalysis*; NanoScience and Technology; Springer: Berlin, 2007.
(76) Jang, T.; Mowbray, D. J.; Dobrin, S.; Falsing, H.; Hvolbaek, B.; Bligaard, T.; Norskov, J. K. *J. Phys. Chem. C* **2009**, *113*, 10548−10553.
(77) Murrell, J. N.; Mottram, R. E. *Mol. Phys.* **1990**, *69*, 571−585.
(78) Noya, E. G.; Doye, J. P. K.; Wales, D. J.; Aguado, A. *Eur. Phys. J. D* **2007**, *43*, 57−60.
(79) The initial structure of the Na_{380} cluster was download from the Cambridge Cluster Database. Wales, D. J.; Doye, J. P. K.; Dullweber, A.; Hodges, M. P.; Naumkin, F. Y.; Calvo, F.; Hernández-Rojas, J.; Middleton, T. F. http://www-wales.ch.cam.ac.uk/CCD.html.
(80) Sánchez-Portal, D.; Ordejón, P.; Artacho, E.; Soler, J. M. *Int. J. Quantum Chem.* **1997**, *65*, 453−461.
(81) Soler, J. M.; Artacho, E.; Gale, J. D.; García, A.; Junquera, J.; Ordejón, P.; Sánchez-Portal, D. *J. Phys.: Condens. Matter* **2002**, *14*, 2745−2779.
(82) Kohn, W.; Sham, L. J. *Phys. Rev.* **1965**, *140*, A1133−A1138.
(83) Cohen, M. L.; Dacorogna, M. M. *Phys. Rev. B* **1986**, *34*, 4996−5002.
(84) Koval, P.; Foerster, D.; Coulaud, O. *J. Chem. Theory Comput.* **2010**, *6*, 2654−2668.
(85) Koval, P.; Foerster, D.; Coulaud, O. *Phys. Status Solidi B* **2010**, *247*, 1841−1848.
(86) Foerster, D.; Koval, P. *J. Chem. Phys.* **2009**, *131*, 044103.
(87) Manjavacas, A.; Marchesin, F.; Thongrattanasiri, S.; Koval, P.; Nordlander, P.; Sánchez-Portal, D.; García de Abajo, F. J. *ACS Nano* **2013**, *7*, 3635−3643.
(88) Mie, G. *Ann. Phys.(Leipzig)* **1908**, *25*, 377−445.
(89) Friedel, J. *Philos. Mag.* **1952**, *43*, 153−189.
(90) Martin, O. J. F.; Girard, C. *Appl. Phys. Lett.* **1997**, *70*, 705−707.
(91) Li, K.; Stockman, M. I.; Bergman, D. J. *Phys. Rev. Lett.* **2003**, *91*, 227402.

DOI: 10.1021/acs.nanolett.5b00759
Nano Lett. 2015, 15, 3410−3419

(92) VKravets, V. G.; Zoriniants, G.; Burrows, C. P.; Schedin, F.; Casiraghi, C.; Klar, P.; Geim, A. K.; Barnes, W. L.; Grigorenko, A. N. *Phys. Rev. Lett.* **2010**, *105*, 246806.
(93) Höpener, C.; Lapin, Z. J.; Bharadwaj, P.; Novotny, L. *Phys. Rev. Lett.* **2012**, *109*, 017402.
(94) Nordlander, P.; Oubre, C.; Prodan, E.; Li, K.; Stockman, M. I. *Nano Lett.* **2004**, *4*, 899−903.
(95) Esteban, R.; Borisov, A. G.; Nordlander, P.; Aizpurua, J. *Nat. Commun.* **2012**, *3*, 825.
(96) Pérez-González, O.; Zabala, N.; Borisov, A. G.; Halas, N. J.; Nordlander, P.; Aizpurua, J. *Nano Lett.* **2010**, *10*, 3090−3095.
(97) Dombi, P.; Hörl, A.; Rácz, P.; Márton, I.; Trügler, A.; Krenn, J. R.; Hohenester, U. *Nano Lett.* **2013**, *13*, 674−678.
(98) Savage, K. J.; Hawkeye, M. M.; Esteban, R.; Borisov, A. G.; Aizpurua, J.; Baumberg, J. J. *Nature* **2012**, *491*, 574−577.
(99) Ding, B.; Deng, Z.; Yan, H.; Cabrini, S.; Zuckermann, R. N.; Bokor, J. *J. Am. Chem. Soc.* **2010**, *132*, 3248−3249.
(100) Pettinger, B.; Schambach, P.; Villagómez, C. J.; Scott, N. *Annu. Rev. Phys. Chem.* **2012**, *63*, 379−399.
(101) Hartschuh, A.; Sánchez, E.; Xie, X.; Novotny, L. *Phys. Rev. Lett.* **2003**, *90*, 095503.
(102) Gerton, J. M.; Wade, L. A.; Lessard, G. A.; Ma, Z.; Quake, S. R. *Phys. Rev. Lett.* **2004**, *93*, 180801.

DOI: 10.1021/acs.nanolett.5b00759
Nano Lett. 2015, 15, 3410−3419